Introducing Dielectrophoresis as a New Force Field for Field-Flow Fractionation

Ying Huang, Xiao-Bo Wang, Frederick F. Becker, and Peter R. C. Gascoyne
Department of Experiment Pathology, University of Texas M. D. Anderson Cancer Center, Houston, Texas 77030 USA

ABSTRACT We present the principle of cell characterization and separation by dielectrophoretic field-flow fractionation and show preliminary experimental results. The operational device takes the form of a thin chamber in which the bottom wall supports an array of microelectrodes. By applying appropriate AC voltage signals to these electrodes, dielectrophoretic forces are generated to levitate cells suspended in the chamber and to affect their equilibrium heights. A laminar flow profile is established in the chamber so that fluid flows faster with increasing distance from the chamber walls. A cell carried in the flow stream will attain an equilibrium height, and a corresponding velocity, based on the balance of dielectrophoretic, gravitational, and hydrodynamic lift forces it experiences. We describe a theoretical model for this system and show that the cell velocity is a function of the mean fluid velocity, the voltage and frequency of the signals applied to the electrodes, and, most significantly, the cell dielectric properties. The validity of the model is demonstrated with human leukemia (HL-60) cells subjected to a parallel electrode array, and application of the device to separating HL-60 cells from peripheral blood mononuclear cells is shown.

INTRODUCTION

The ability to characterize, separate, and purify cell subpopulations is fundamental to numerous biological and medical applications, often forming the starting point for research protocols and the basis for current and emerging clinical protocols. For example, cell separation can make possible life-saving procedures such as autologous bone marrow transplantation for the remediation of advanced cancers, where the removal of cancer-causing metastatic cells from a patient's marrow is necessary (Fischer, 1993). Another example is blood cell differential analysis, which is a common procedure in clinical and research laboratories. Current approaches to cell sorting most frequently exploit differences in cell density (Boyum, 1974), specific immunological targets (Smeland et al., 1992), or receptor-ligand interactions (Chess and Schlossman, 1976) to isolate target cells. These techniques are often inadequate, and sorting devices capable of identifying and selectively manipulating cells through novel physical properties are therefore desirable.

Electrical-field-induced forces on polarizable particles have been the subject of extensive studies in recent years because of their potential applications for particle characterization and manipulation. Particles, including biological cells, become electrically polarized under the influence of applied fields. The induced polarizations can in turn interact with applied fields, resulting in net electrical forces on the particles. Because of the sensitive dependence of these forces on particle dielectric characteristics, these forces can be exploited for particle characterization and separation. Even though Pohl (1977) proposed 20 years ago the pioneering idea of utilizing the difference between dielectrophoretic (DEP) forces exerted on different particles in nonuniform electric fields for sorting applications, DEP phenomena were not effectively exploited for this purpose until, in recent years, the theoretical understanding of DEP effects improved and microelectrode arrays were introduced. Two approaches have been demonstrated for DEP separation: namely DEP migration and DEP retention. DEP migration exploits opposing polarities of DEP forces exerted on different particle types, so that one type is attracted toward high-field regions by positive dielectrophoresis while the other type(s) are repelled by negative dielectrophoresis. In this way, different particle types are focused at different regions of a microelectrode structure and spatial separation is achieved (Gascoyne et al., 1992; Wang et al., 1993; Markx et al., 1994a). DEP retention exploits competition between DEP and fluid-flow forces. Particles experiencing a weaker DEP force (negative or small positive) are eluted by fluid flow, whereas particles experiencing strong positive DEP forces are trapped at electrode edges against the drag of the fluid flow (Wang et al., 1993; Markx et al., 1994b). Using this approach, Becker et al. (1994, 1995) achieved separation of leukemia and breast cancer cells from blood under appropriate electrical field and fluid flow conditions. Talary et al. (1995) reported a different version of DEP retention wherein DEP trapping forces on cells were gradually decreased by lowering the frequency of the excitation voltage while maintaining a constant fluid flow rate. At each field frequency (applied for 10 min), the DEP forces acting on a given subpopulation of cells became smaller than the fluid drag forces, so that this subpopulation was released, eluted, and collected. This allowed a sixfold enrichment to be achieved of CD34+ stem cells from peripheral blood (Talary et al., 1995). More recently, Markx and

Received for publication 21 February 1997 and in final form 21 April 1997.

Address reprint requests to Dr. Peter R. C. Gascoyne, Department of Experiment Pathology, Box 89, University of Texas M. D. Anderson Cancer Center, 1515 Holcombe Boulevard, Houston, TX 77030. Tel.: 713-792-4534; Fax: 713-792-5940; E-mail: peter@solace.mdacc.tmc.edu.

0006-3495/97/08/1118/12 $2.00

Pethig (1995) reported a continuous separation technique for separating viable and nonviable cells based on DEP retention. Both the DEP migration and DEP retention methods depend upon there being relatively large differential DEP forces between the particle types being sorted, and thus it is difficult to separate mixtures of cell subpopulations with small dielectric differences. The present paper presents an approach to solving this problem.

Since the 1960s there has been interest in a family of techniques collectively termed field-flow fractionation (FFF), wherein the velocity gradient of a hydrodynamic flow profile is exploited to achieve particle fractionation (Giddings, 1993). In these techniques, a laminar fluid profile is established in a thin chamber, such that fluid moves faster with increasing distance from the chamber walls. By applying a force field perpendicular to the flow direction and across the flow profile, particles are forced toward a so-called accumulation wall (typically the bottom wall) of the chamber. In normal-mode FFF, particles are sufficiently small (<1 μm) that the diffusion and accumulation forces counteract, and an equilibrium concentration profile results along the force-field direction and hence across the fluid velocity profile. Particles are thereby carried by the fluid at velocities that depend on their equilibrium profile. Dissimilar particle types exhibit different characteristic concentration profiles, are carried at different velocities, and hence take different times to traverse the separation chamber. Therefore they can be separated by collecting them at appropriate times at the chamber exit. Typically in the normal FFF mode, small particles are eluted before large ones. In the second mode of FFF, the imposed force field is so strong and diffusion forces are sufficiently suppressed, that particles (typically 1–200 μm in diameter) are instead forced against the accumulation wall, where the fluid velocity is low and steric hindrance to flow takes place. In this so-called steric-FFF mode, larger particles typically are eluted first because of the larger fluid drag forces they experience. A third type of FFF, an extension of steric mode, is lift-hyperlayer FFF, in which the imposed force field is used to balance the hydrodynamic lift force from the fluid flow. This lift force is strong close to the chamber walls, and particles with different properties become positioned at different equilibrium heights from the chamber wall in the flow profile and are therefore eluted at different velocities.

FFF has been successfully employed for analysis and fractionation of macromolecular, colloidal, and particulate materials with different force mechanisms such as sedimentation, cross-flow, thermal diffusion effects, and electrophoresis (Giddings, 1989; Cardot et al., 1994). Separation of cells and cellular components has been reported in biomedical applications (Berg and Turner, 1991; Litzen et al., 1993; Mosersky et al., 1988). Nevertheless, a major factor limiting further FFF development was the lack of an effective force mechanism for sensitively controlling the equilibrium positions of particles throughout the flow profile based on differences in their intrinsic properties. For lift-hyperlayer FFF, fractionation relies on establishing an equilibrium between the imposed field and hydrodynamic lift. Typically the imposed field is spatially homogeneous, and equilibrium is achieved by balancing it against the inhomogeneous lift force. This is not ideal for cell separation applications, because the lift force falls off rapidly with height above the accumulation well and depends mainly on particle size. This results in limited discriminatory ability between particle types.

Here we introduce the concept of balancing spatially inhomogeneous dielectrophoretic levitation forces with homogeneous gravitational forces as a means of controlling the heights of particles for FFF applications (Gascoyne et al., 1996). Thus we combine dielectrophoretic levitation of particles (Kaler and Jones, 1990; Fuhr et al., 1992) with FFF concepts to provide a versatile separation method. In this article we present a theoretical description of this dielectrophoretic field-flow fractionation (DEP-FFF) technique and demonstrate its validity with a simple, biologically relevant experimental model.

DEP-FFF THEORY

Consider a thin chamber constructed with a bottom wall that supports a planar electrode array. Under AC electrical excitation, the array will produce height-dependent dielectrophoretic forces on particles in the chamber. The vertical component of the DEP force averaged along a horizontal plane at a height h above the electrode plane that acts on a particle of radius r can be written as (Jones, 1979; Wang et al., 1995)

$$F_{\mathrm{DEP}_z} = 2\pi\epsilon_m r^3 \mathrm{Re}(f_{\mathrm{CM}})\langle \nabla E_{\mathrm{RMS}}^2 \cdot \vec{a}_z \rangle = 2\pi\epsilon_m r^3 p \mathrm{Re}(f_{\mathrm{CM}}) q(h) U^2 \quad (1)$$

where E_{RMS} is the RMS value of the field strength for an applied RMS voltage U, and $\mathrm{Re}(f_{\mathrm{CM}})$ is the real component of f_{CM}, the Clausius-Mossotti factor. f_{CM} reflects the magnitude and direction of field-induced polarization in the particle at frequency f, and is given by $f_{\mathrm{CM}} = (\epsilon_p^* - \epsilon_m^*)/(\epsilon_p^* + 2\epsilon_m^*)$, where ϵ_p^* and ϵ_m^* are the frequency-dependent complex dielectric permittivities of the particle and its suspending medium. The function $q(h)$ reflects the height dependence of the vertical DEP force component, which decreases with increasing height. Because electrode polarization causes a frequency-dependent voltage drop at the electrode/solution interface (Schwan, 1992; Zhou et al., 1995; Wang et al., 1997), we have also introduced the function p ($p(f)$) to correct for its effect on DEP forces.

The idea is to use DEP forces to levitate and position particles at equilibrium heights that reflect their dielectric properties. Thus particles with dielectric differences will, in general, attain different equilibrium positions. At equilibrium, the DEP and sedimentation forces acting on a particle will balance, so that

$$-\frac{4}{3}\pi r^3(\rho_p - \rho_m)g + F_{\mathrm{DEP}_z} = 0, \quad (2)$$

where g is the acceleration due to gravity, and ρ_p and ρ_m are the densities of the particle and its suspending medium, respectively. Combining Eqs. 1 and 2, we obtain

$$2(\rho_p - \rho_m)g = 3\epsilon_m p\mathrm{Re}(f_{CM})q(h_{eq})U^2 \quad (3)$$

whence the equilibrium height follows as

$$h_{eq} = q^{-1}\left(\frac{2(\rho_p - \rho_m)g}{3\epsilon_m p\mathrm{Re}(f_{CM})U^2}\right) \quad (4)$$

where $q^{-1}(h)$ is the inverse of $q(h)$. Equation 4 shows that particle levitation is determined by the relative particle density $(\rho_p - \rho_m)$, the particle dielectric property $\mathrm{Re}(f_{CM})$, the field distribution $q(h)$ in the vertical direction, the applied voltage U, and the electrode polarization function $p(f)$.

If a laminar flow profile is now established in the chamber, the fluid velocity v_f at a height h above the bottom wall follows a hyperbolic function:

$$v_f = 6\langle v\rangle\frac{h}{H}\left(1 - \frac{h}{H}\right) \quad (5)$$

where H is the chamber thickness and $\langle v\rangle$ is the mean fluid velocity. A particle of radius r located at a height h from the chamber bottom wall in this flow profile will be carried along at a velocity v_p, given (Williams et al., 1992) as

$$v_p = v_f \cdot k_r \quad (6a)$$

where

$$k_r = 1 - \frac{5}{16}\left(\frac{r}{h}\right)^3 \qquad \text{for } h > 1.1r$$

and

$$k_r = \frac{0.74}{0.5 - 0.2\log((h - r)/r)} \qquad \text{for } h < 1.1r \quad (6b)$$

Here k_r (< 1) is a coefficient that characterizes the retardation effect that occurs as the particle approaches the chamber wall. In addition to the dielectrophoretic and gravitational forces in Eq. 2, the equilibrium height of a particle in the fluid-flow profile will be affected by the hydrodynamic lifting force F_{lift}, given by

$$h_{eq} = q^{-1}\left(\frac{2(\rho_p - \rho_m)g - 3F_{lift}/(2\pi r^3)}{3\varepsilon_m p\mathrm{Re}(f_{CM})U^2}\right) \quad (7)$$

A number of theoretical studies have addressed the hydrodynamic lifting effect, and several physical mechanisms for F_{lift} have been proposed, including the fluid inertial effect (Cox and Hsu, 1977), shear-stress gradient-induced lift (Leighton and Acrivos, 1985), and lubrication theory (Goldman et al., 1967). Nevertheless, the lifting forces predicted from all of these theories are much smaller than those observed experimentally (Williams et al., 1992). Although the nature of the lifting force remains in question, Williams et al. (1992) have determined its dependency on the chamber thickness H, particle position h, radius r, mean fluid velocity $\langle v\rangle$, and fluid viscosity η, based on the experimental data for artificial polystyrene beads, and presented the empirical relationship

$$F_{lift} = C\frac{6\eta r^3\langle v\rangle}{H(h - r)} \quad (8)$$

where C ($= 0.172$) is a constant.

The operational principle of DEP-FFF can be summarized as follows. By applying appropriate voltage signals to the electrodes, particles with different dielectric and/or density properties can be levitated to different heights (Eq. 7) and thereby caused to move at different velocities under the influence of the flow profile (Eqs. 5 and 6, Fig. 1). Particles preloaded at the chamber inlet will then exit the chamber at different times, so they can be collected separately. In this way, the times taken for particles to transit the chamber directly reflect their dielectric and density properties, and this dependency can be utilized for particle characterization and separation. The fact that the velocity gradient in the flow profile is actively exploited for DEP-FFF constitutes the main difference from the DEP retention method. In the DEP retention method, all particles stay on the same plane, and depending on the competition of the horizontal fluid drag and DEP forces, they are either eluted from the chamber or trapped at the electrode edges until the electrical forces are removed or made weak enough to release them. In contrast, in DEP-FFF, particles are positioned in different planes throughout the hydrodynamic flow profile above the electrode surface as a result of the balance between sedimentation, vertical DEP, and hydrodynamic-lift forces. Thus particles are eluted in a continuous fashion at different velocities under the influence of horizontal fluid drag acting in their respective planes. In this way, DEP-FFF utilizes the full range of fluid velocities within the flow profile and, more importantly, exploits the three-dimensional capacity of the separation chamber. This tends to limit particle-particle interactions (Becker et al., 1995) that occur when the particles are confined largely to a single active plane, as in the DEP retention approach to separation, because the mean distance between cells in DEP-levitation is increased as they are spread out vertically above the electrode plane.

To demonstrate the dependencies of particle height and velocities on particle dielectric properties and on the voltage and frequency of the applied field as predicted in the above equations, we shall present experimental data for human leukemia HL-60 cells on a parallel electrode system. Furthermore, we shall apply DEP-FFF to separate human leukemia HL-60 cells from peripheral blood mononuclear cells as an example of cell fractionation.

MATERIALS AND METHODS

Cells

The human leukemia HL-60 cell line was used as a model system in this study. Cells were cultured in RPMI 1640 medium supplemented with 10%

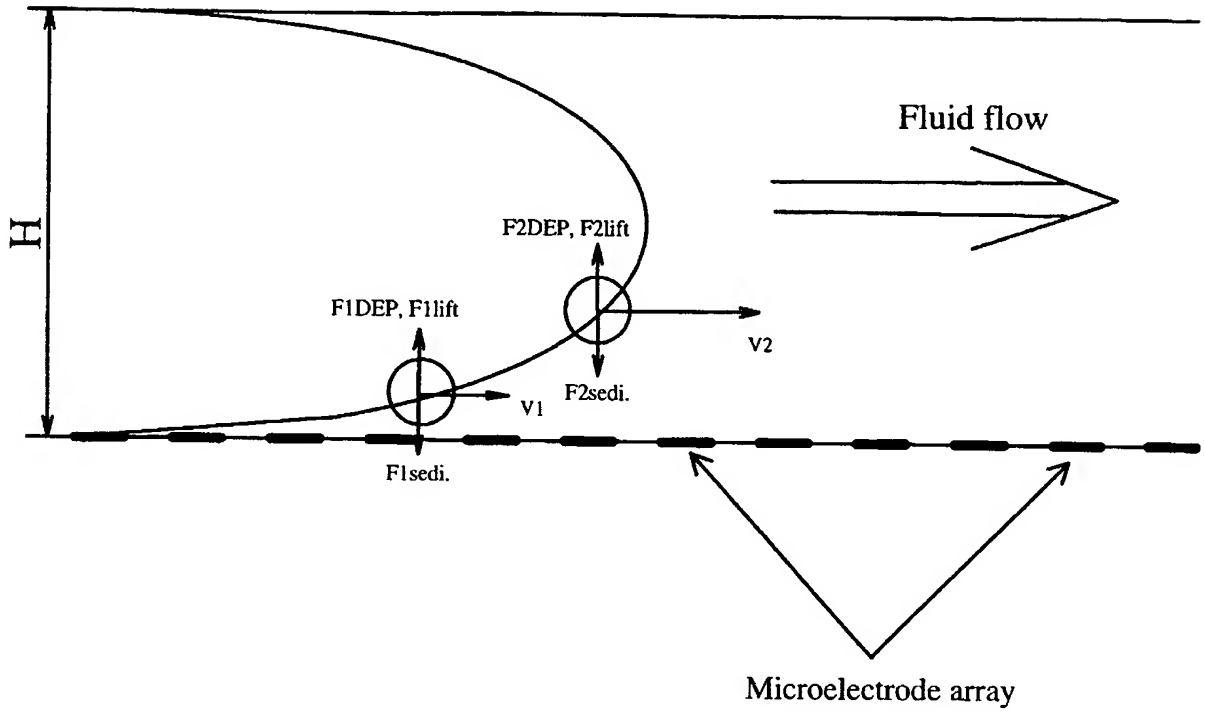

FIGURE 1 Schematic diagram outlining the DEP-FFF principle. A fluid flow profile is established in a thin chamber whose bottom plane supports a microelectrode array. Two particles of different dielectric properties equilibrate at different heights under the balance of DEP levitation, hydrodynamic lift, and sedimentation forces. Particle 2, being levitated further away from the chamber bottom wall, exhibits a larger velocity under the influence of fluid drag than particle 1.

fetal bovine serum, 1 mM glutamine, and 20 mM HEPES (Life Technologies, Gaithersburg, MD), 0.5% penicillin, and streptomycin solution (Sigma, St. Louis, MD), and were maintained in 75-cm^2 plastic flasks under a 5% CO_2/95% air atmosphere at 37°C in a humidified incubator. HL-60 cells were harvested at a density of 2×10^6/ml in the exponential growth phase by gently rocking the flask 48 h after seeding. Cell suspensions were found to have >98% viability by Trypan blue dye exclusion. Cells were harvested from complete medium by centrifugation at $100 \times g$ for 10 min and were then resuspended at a density of $\sim 10^6$/ml in isotonic 8.5% (w/v) sucrose plus 0.3% (w/v) dextrose buffer. The conductivities of the final suspensions were adjusted with culture medium to a nominal value of 50 mS/m, and were then measured with a conductivity meter (EC19101-00; Cole-Parmer Instrument, Chicago, IL). Peripheral blood mononuclear (PBMN) cells were prepared from a buffy coat by standard density gradient separation (Boyum, 1974). To quantify cell levitation effects, the specific densities of HL-60 cells were assessed to be 1.071 ± 0.003 g/cm^3 with centrifugally generated continuous Percoll density gradients (Pharmacia, Uppsala, Sweden) calibrated by Percoll density marker beads. The specific density of the cell suspending medium was measured to be 1.033 g/cm^3 with a hydrometer (VWR Scientific, Greenbelt, MD).

Electrode chambers

Parallel electrode arrays, shown in Fig. 2, were fabricated by standard photolithography. In brief, gold-coated (thickness 250 Å over a 100-Å titanium seeding layer) glass blanks (Thin Film Technology, Buellton, CA) were spin-coated at 3000 rpm with S1830 photoresist (Shipley, Marlborough, MA) to ~ 1 μm thickness. The photoresist was polymerized by baking on a hot plate at 110°C for 1 min and then exposed to UV light through a positive mask image (Process Technologies, Oak Creek, WI) of the electrode array, using a mask aligner (AB Manufacturing, San Jose, CA). The exposed photoresist was developed with MF351 developer, and the exposed gold-and-titanium region was then etched. Finally, the photoresist covering the unetched regions of the electrodes was removed with acetone. Arrays of parallel electrode elements with equal widths and gaps of 20 and 50 μm were both used in this study.

FFF chambers of dimensions 200 μm (H) × 25 mm (L) × 17 mm (W) were constructed of parallel top and bottom glass plates separated by a Teflon spacer, as shown in Fig. 2. The arrays of parallel electrodes were on the inner surface of the bottom plates. Polyethylene tubes (ID 0.87 mm; OD 1.22 mm), glued into holes drilled through the top glass plate with a diamond drill, allowed for the introduction and removal of cell suspensions and eluate buffer.

Cell DEP-FFF kinetics

After the introduction of a cell sample into the chamber inlet, cells were allowed to settle on the electrode plane for ~20 s before the application of electrical signals. Sinusoidal voltages between 10 kHz and 1 MHz and up to 3 V (RMS) from a function generator (HP33120; Hewlett Packard, Santa Clara, CA) were then applied to the electrode elements through coaxial cables, and fluid flow was started by pumping the sucrose/dextrose buffer through the inlet port with a digital syringe pump (Daigger, Wheeling, IL) at flow rates of 20, 40, or 80 μl/min. Cell kinetic behaviors were viewed by looking up through the chamber bottom with a Nikon (Melville, NJ) TMD inverted microscope equipped with a Hamamatsu (Bridgewater, NJ) CCD video camera and recorded on videotape. Long working-length objective lenses of 4× to 40× provided final magnifications of between 140 and 1400 on the TV monitor. Cell velocities were analyzed by measuring the time taken for individual cells to move at least 120 μm (≥ 3 electrode + gap periods). In cell levitation experiments, the fluid flow was stopped, and heights of the cells above the electrode plane were measured to an accuracy of ±2 μm, by subtracting the corresponding readings on the focusing dial when focusing first on the electrode plane and

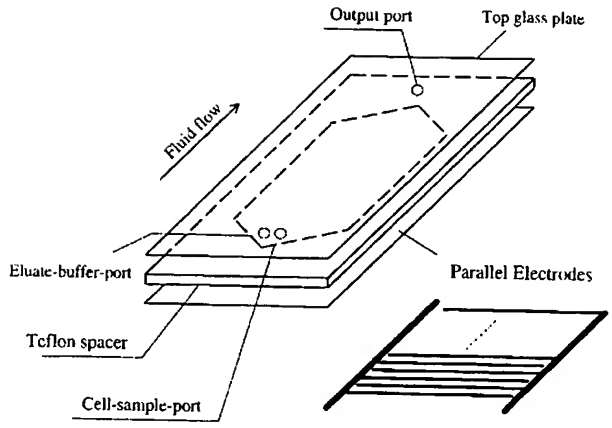

FIGURE 2 Schematic representation of a DEP-FFF chamber of dimension 200 μm (H) × 25 mm (L) × 17 mm (W). The cell sample is preloaded into the inlet regions of the chamber from the cell sample port. After cells settle onto the bottom wall, eluate buffer is pumped through the chamber via the eluate buffer port to establish a hydrodynamic laminar flow profile in the chamber. Appropriate voltage signals are then applied to the electrode elements to cause cells to equilibrate at different heights and travel at correspondingly different velocities in the flow profile. In this study, parallel electrodes with equal electrode width and spacing of 20 (or 50) μm were used with alternate elements connected to electrode buses running along the two long edges of the chamber.

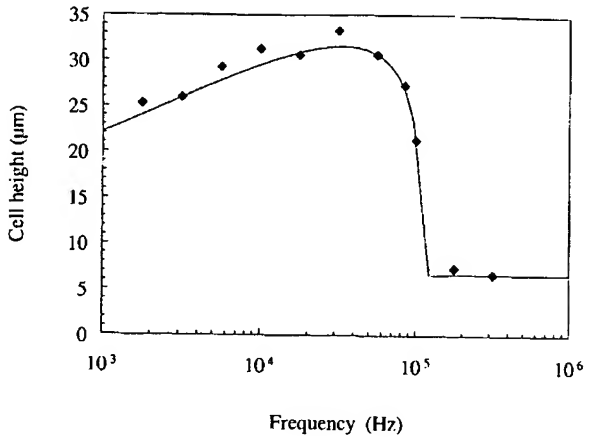

FIGURE 3 Frequency dependency of levitation height (◆) of a typical HL-60 cell (radius 6.6 μm) suspended in a sucrose/dextrose medium of conductivity 56 mS/m under an applied voltage of 1.06 V (RMS) on a parallel electrode array (20 μm width and spacing). No fluid flow is present. The continuous curve represents the best fit of the experimental data using Eq. 10, where the factor $\mathrm{Re}(f_{CM})$ is based on a single-shell dielectric model (Irimajiri et al., 1979; Huang et al., 1992), for which the cell interior relative permittivity and conductivity are assumed to be 75 and 0.75 S/m, respectively. The best fit yielded values for the membrane capacitance and conductance of 16.3 mF/m^2 and <50 S/m^2, respectively.

then on the cells and correcting for the refractive index (1.33) of the suspending medium.

RESULTS

DEP levitation

Fig. 3 shows the typical frequency dependency of levitation height for HL-60 cells at a suspension conductivity of 56 mS/m for an applied voltage of 1.06 V (RMS). As the frequency of the voltage was increased from 2 to 30 kHz, the cell levitation height steadily rose. However, increasing the frequency above 30 kHz led to a sharp drop-off in levitation height, until the cell became trapped at the electrode edges above 300 kHz. The levitation characteristics of other cell types, including murine erythroleukemia DS19 and human breast cancer MDA-MB-231 cells (data not shown), exhibited qualitatively similar frequency dependencies, except that the sharp transition from cell levitation to trapping occurred in characteristically different frequency ranges for each cell type. Fig. 4 shows the typical voltage dependency of HL-60 levitation at a frequency of 17.8 kHz. Clearly, the levitation height exhibited a sublinear, monotonic relationship to the applied voltage.

DEP-FFF velocity

The effectiveness of applying DEP forces to control particle velocities in a fluid flow profile was studied by measuring the velocities of HL-60 cells in a DEP-FFF chamber as a function of the frequency and magnitude of the signals applied to the electrode array. It was not possible to measure these dependencies for single cells because of the impracticality of tracking them throughout an entire experiment. Instead, the velocities of ~20 individual cells chosen at random were determined for each experimental condition. Fig. 5 illustrates the frequency dependencies of the mean velocity of HL-60 cells for three different rates of fluid flow. Cells moved faster with increasing flow rate; thus at

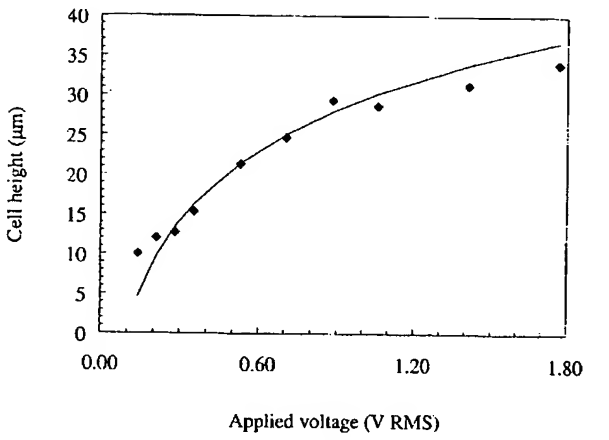

FIGURE 4 The voltage dependency of the levitation height (◆) of an HL-60 cell (radius 6.3 μm) suspended in a medium of conductivity 56 mS/m for an applied field of frequency 17.8 kHz. No fluid flow is present. The continuous curve represents the best fit of Eqs. 10 and 13 to the experimental data, whence the factor $\mathrm{Re}(f_{CM})$ is derived as −0.43. In the simulation, the value for the electrode polarization factor $p(f)$ at 17.8 kHz was 0.67, as taken from Fig. 8 (see text). The parameter h_0 in Eq. 13 was determined to be 29.5 μm.

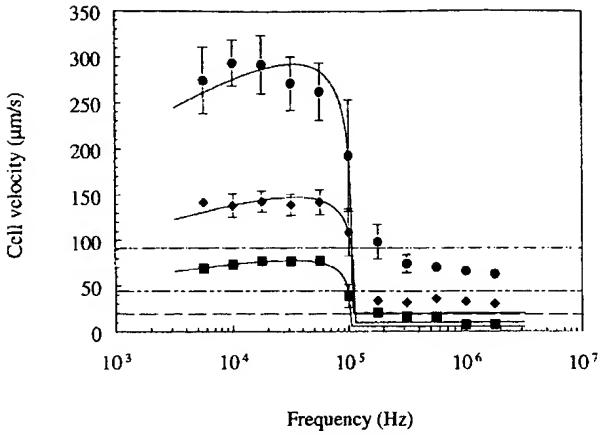

FIGURE 5 The frequency dependency of the mean velocity for HL-60 cells suspended in a sucrose/dextrose medium of conductivity 44 mS/m in a thin chamber containing parallel microelectrode arrays (20 μm width and spacing) at flow rates of 20 (■, $\langle v \rangle$ = 98); 40 (◆, $\langle v \rangle$ = 196); and 80 μl/min (●, $\langle v \rangle$ = 392 μm/s). The applied voltage was 1.06 V (RMS). Chamber dimensions were 200 μm (H) × 25 mm (L) × 17 mm (W). Each symbol represents the mean velocity of ~20 cells. The continuous lines show the best fit of Eq. 10, the broken lines (20 μl/min, — —; 40 μl/min, — · · —; 80 μl/min, — · — ·) the averaged cell velocity when the electrical field was turned off. In the single shell model, the cell radius, interior relative permittivity, and conductivity are taken to be 5.8 μm (measured by microscopy), 75, and 0.75 S/m, respectively. The best fits for the three flow rates gave values for cell membrane-specific capacitance of 15.6 (± 0.95) mF/m^2 and conductance of 220 (± 76) S/m^2.

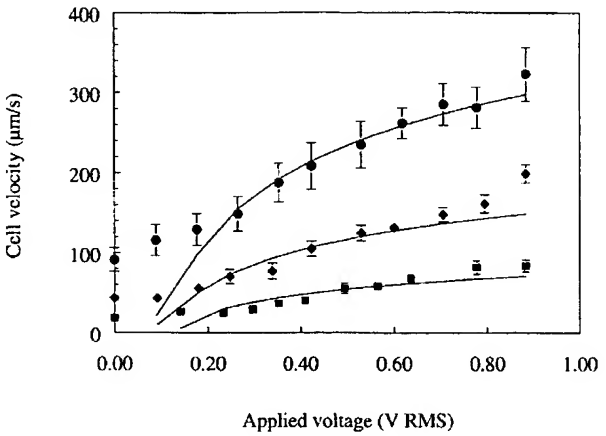

FIGURE 6 Voltage dependency of the mean velocity of HL-60 cells suspended in a sucrose/dextrose medium of conductivity 44 mS/m in a thin chamber containing parallel microelectrode arrays (20 μm width and spacing) at flow rates of 20 (■, $\langle v \rangle$ = 98), 40 (◆, $\langle v \rangle$ = 196), and 80 μl/min (●, $\langle v \rangle$ = 392 μm/s). The applied field frequency was 31.6 kHz. Chamber dimensions were 200 μm (H) × 25 mm (L) × 17 mm (W). The continuous curve represents a best fit of Eq. 10 to the experimental data, for which the factor Re(f_{CM}) was derived as −0.46 (± 0.065).

an applied frequency of 17.8 kHz, the mean velocity increased from 77 (± 4.1) to 292 (± 32) μm/s as the flow rate was varied from 20 to 80 μl/min. The overall frequency dependency did not appear to change with the flow rate, and application of voltage signals caused HL-60 cells to move at either higher or smaller velocities. For a flow rate of 20 μl/min, in the applied frequency range of 10–50 kHz, cell velocities were about four times higher than they were with no field applied. In the narrow frequency band from 100 to 300 kHz, cell velocities decreased sharply to those observed with no field applied. At 100 kHz, individual HL-60 cells exhibited vastly different velocities, and fast-moving cells traveled five times faster than the slowest ones. Under these conditions, the variance of cell velocities was ~30%, in contrast to ~10% for frequencies below 100 kHz. Increasing the field frequency above 300 kHz resulted in a further decrement in mean velocity to values much smaller than those observed in the absence of an electrical field. For example, at 1 MHz, the mean velocities were ~40% and 73% of the zero-field values for flow rates of 20 and 80 μl/min, respectively. For the small flow rate of 20 μl/min, some HL-60 cells were even trapped on electrode edges.

The voltage dependencies of the mean velocity are shown in Fig. 6 for HL-60 cells at a fixed frequency of 31.6 kHz for three different flow rates, and as in Fig. 5, increasing the flow rate led to faster cell elution. For a given flow rate, the mean velocity increased steadily with applied voltage.

Separation of HL-60 cells from peripheral blood mononuclear cells

Two approaches, namely DEP retention and DEP-FFF, were used to separate HL-60 cells from a mixture with PBMN cells in a parallel electrode chamber. The device was the same as in Fig. 2, except that it had dimensions of 375 μm (H) × 150 mm (L) × 24 mm (W) and electrode widths and spacings of 50 μm. Cell mixtures in the ratio of 1:5 for HL-60:PBMN cells (predominately lymphocytes) were prepared in isotonic sucrose/dextrose buffer containing 10^6 HL-60 cells/ml at a conductivity of 10 mS/m. About 250 μl of cell mixture was loaded into the chamber with a syringe for each separation experiment, and cells were allowed to settle on the electrode plane for ~20 s. For DEP retention, signals of 0.88 V (RMS) at 50 kHz were then applied to the electrode arrays, while the sucrose/dextrose eluate buffer was pumped through the chamber at a flow rate of 160 μl/min. All HL-60 cells were trapped at the electrode edges, while PBMN cells were carried away with the fluid and were collected at the chamber outlet. The voltage was then switched off to release the HL-60 cells, which were subsequently collected.

For DEP-FFF, voltage signals of 25 kHz and 0.88 V (RMS) were applied to the electrode arrays, and an eluate flow in the chamber was established at a rate of 160 μl/min. Almost all of the PBMN cells and HL-60 cells were levitated and were caused to move under the influence of the fluid. Using the significant difference in cell size as the basis for identification, it was observed that PBMN cells were levitated to higher positions and traveled about twice as fast as HL-60 cells. Therefore PBMN cells were eluted from the chamber in about half the time (15 min) taken by

HL-60 cells (26 min), and excellent separation was thereby obtained.

DISCUSSION

DEP levitation

To analyze the cell levitation characteristics, we determined the field distribution of parallel electrode arrays by using both the charge density method (Sadiku, 1996) and the Green's theorem-based method (Wang et al., 1996). The two analyses gave similar results, and a vector representation of the DEP force distribution for a plane normal to parallel electrodes is shown in Fig. 7. It was found that the vertical DEP component averaged over horizontal planes parallel to the electrode surface exhibited an approximately exponential decay with height h, so that the function $q(h)$ in Eq. 1 can be approximated as

$$q(h) = A\exp(-4\pi h/d) \tag{9}$$

where A is a constant and d is the periodic distance (d = 80 μm, $A = -2.77 \times 10^{14}$ m^{-3} for parallel electrodes of 20 μm width and spacing) of the parallel electrode array. Combining Eqs. 4 and 9, we can then express the equilibrium height of a cell as

$$h_{eq} = \frac{d}{4\pi}\left(2\ln(U) + \ln(ApRe(f_{CM})) + \ln\left(\frac{3\epsilon_m}{2(\rho_c - \rho_m)g}\right)\right) \tag{10}$$

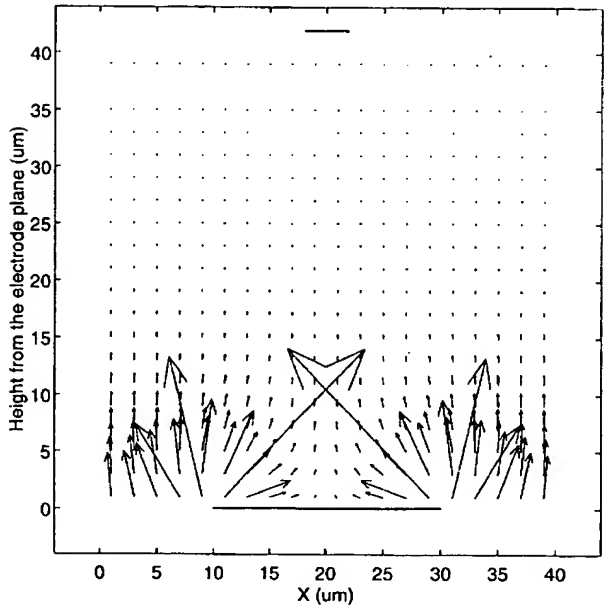

FIGURE 7 Vector representation of the DEP forces acting on a cell of radius 5.8 μm for a plane normal to parallel electrodes (electrodes are represented by the bold line at z = 0) for an applied voltage of 1 V (RMS). Parameter Re(f_{CM}) was assumed to be −0.5 for the calculation. Scale bar = 500 pN.

Using Eq. 10, we simulated the frequency dependencies of cell levitation height. For this simulation, the electrode-polarization function $p(f)$ was determined through analysis of experimental impedance data. Electrode polarization (Schwan, 1992) is an effect associated with the discontinuity in current carriers at the electrode/solution interface. Such a discontinuity leads to a frequency-dependent potential drop across the interface, causing the voltage impinging on the bulk solution to be smaller than that applied to the electrodes. To quantify this effect in terms of $p(f)$, we measured the total impedance of the electrode system as a function of the applied frequency and fitted the data to an ion-diffusion-based model for electrode polarization. This model assumes that the polarization capacitance and resistance are both proportional to $f^{-0.5}$ and that the impedance has a frequency-independent phase angle (Schwan, 1992). The total impedance of the system is then given by

$$Z_{total} = Z_{bulk} + Z_{pol} = \frac{R_{bulk}}{1 + i2\pi f R_{bulk}C_{bulk}} + \left(R_0 f^{-0.5} + \frac{i}{wC_0 f^{-0.5}}\right) \tag{11}$$

where the resistance (R_{bulk}) and capacitance (C_{bulk}) of the bulk solution are in parallel, and the resultant bulk impedance (Z_{bulk}) is in series with the polarization resistance ($R_0 f^{-0.5}$) and capacitance ($C_0 f^{-0.5}$). Analysis of the experimental data for the frequency dependence of Z_{total} based on Eq. 11 allowed us to determine the polarization parameters (R_0 = 652 $\Omega \cdot$ Hz$^{0.5}$ and C_0 = 6.5 mF $\cdot$ Hz$^{0.5}$ for a 5.75-cm^2 parallel electrode array of 20 μm width and spacing) and, in turn, to calculate the polarization function $p(f)$ as

$$p(f) = \frac{U_{eff}}{U_{appl}} = \frac{Z_{bulk}}{Z_{total}} = \frac{R_{bulk}}{(1 + i2\pi f R_{bulk}C_{bulk})(Z_{bulk} + Z_{pol})} \tag{12}$$

The frequency dependency of the polarization function $p(f)$ is shown in Fig. 8. For a bulk-solution conductivity of 56 mS/m, more than 40% of the applied voltage was dropped at the polarization interface at a frequency of 10 kHz, and it was only above 25 kHz that more than 90% of the applied voltage was available to produce dielectrophoretic forces within the chamber. Thus electrode polarization accounts for the increment of the cell levitation height in the frequency range 2–30 kHz observed in Fig. 3. At frequencies above 50 kHz, the polarization effect was negligible, and the sharp drop-off in the levitation height observed above 50 kHz resulted from the decrement of the parameter Re(f_{CM}) (see Fig. 10). Combining Eqs. 10 and 12, we performed a best fit of frequency-dependence data of the levitation height to a single-shell dielectric model (Irimajiri et al., 1979; Huang et al., 1992) of HL-60 cells. Good agreement between experiment and theory was found, as evidenced by the fact that the regression coefficient for fitting (defined as

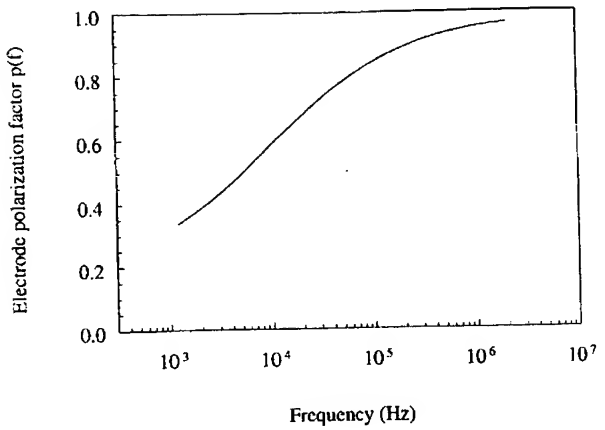

FIGURE 8 The frequency dependency of the electrode polarization function $p(f)$ expressing the proportion of the voltage applied to the electrode array that impinges on the bulk solution to give rise to DEP forces. The electrical conductivity of the bulk solution was 56 mS/m.

$(1 - \Sigma_i(h_{\text{theoretical}}(f)_i - h_{\text{experimental}}(f_i))^2/\Sigma_i h^2_{\text{experimental}}(f_i)))$ was typically >0.99.

For a fixed applied field frequency, and thus a constant value of $\text{Re}(f_{\text{CM}})$, the equilibrium height of cells exhibited a logarithmic dependence on the applied voltage:

$$h_{\text{eq}} = \frac{d}{2\pi} \ln U + h_0 \tag{13}$$

where h_0 is a constant that corresponds to the levitation height at an applied voltage $U = 1$ V at fixed values of $\text{Re}(f_{\text{CM}})$, $p(f)$, ρ_c, and ρ_m (see Eq. 10). Thus the levitation height h_{eq} increased with the applied voltage U, and the incremental slope was inversely proportional to U. By fitting Eq. 13 to the experimentally observed voltage dependence of levitation height, we were able to derive values of $\text{Re}(f_{\text{CM}})$ for different cells at each applied frequency. Although, as shown in Fig. 4, reasonable fits were obtained (regression coefficient = 0.99), the levitation heights predicted from Eq. 13 were consistently smaller than the experimentally observed values for small applied voltages ($\leq$ 0.2 V (RMS)). We believe that this discrepancy arose because the theoretical treatment of Eq. 13 is based solely on dipole-derived forces and ignores force contributions from higher order polarization (Washizu and Jones, 1996).

DEP-FFF velocity

Combining Eqs. 5, 6, and 10, we obtain the particle velocity in a DEP-FFF chamber:

$$v_p = \frac{3k_t\langle v\rangle d}{2\pi H}\left(2\ln(U) + \ln(Ap\text{Re}(f_{\text{CM}})) + \ln\left(\frac{3\epsilon_m}{2(\rho_c - \rho_m)g}\right)\right) - \frac{3k_t\langle v\rangle d^2}{8\pi^2 H^2}\left(2\ln(U) + \ln(Ap\text{Re}(f_{\text{CM}})) + \ln\left(\frac{3\epsilon_m}{2(\rho_c - \rho_m)g}\right)\right)^2 \tag{14}$$

However, as discussed earlier, particles traveling in a DEP-FFF chamber experience hydrodynamic lift forces in addition to the DEP-levitation and gravitational forces that are taken into account in Eq. 14. The hydrodynamic lift effect is evidenced by the fact that the mean velocities of HL-60 cells, when no electrical field was applied, were 23.1 ($\pm$2.3), 48.5 ($\pm$6.8), and 99.5 ($\pm$16.2) μm/s for flow rates of 20, 40, and 80 μl/min, respectively, more than twice than those (10.1, 20.2, and 40.4 μm/s) predicted under the assumption that cells settled to just 0.1 μm above the electrode plane. Assuming an average cell radius of 5.8 μm, Eqs. 5 and 6 show that the cell centers must have been levitated by the lift forces to average heights of 9, 9.4, and 9.7 μm (corresponding to the distance between cell surfaces and the electrode plane of 3.2, 3.6, and 3.9 μm), to attain their observed velocities for flow rates of 20, 40, and 80 μl/min, respectively. Using these estimated heights and Eq. 8, we determined the corresponding lift forces. It was found that the equilibrium lift force at a flow rate of 80 μl/min was 3.4 times higher than for a flow rate of 20 μl/min. This is incompatible with the fact that the equilibrium hydrodynamic lift force must always equal the sedimentation force and be independent of the flow rate. This discrepancy may have resulted from the fact that both Eqs. 6 and 8 are based on experimental data for smooth polystyrene beads and may not be applicable to the rough HL-60 cells studied here. To accurately analyze DEP-FFF performance, we are therefore currently investigating this hydrodynamic lifting effect for mammalian cells, and special attention is being paid to the influence on the lifting force of thermal convection generated by applied-field-dependent Joule-heating. Thus although it is clear that the equilibrium positions of cells within our DEP-FFF chamber were determined, as embodied in Eq. 7, by the balance between DEP-levitation, the hydrodynamic lift, and sedimentation forces, a lack of knowledge of the precise nature of the hydrodynamic lift component renders Eq. 14 inadequate and currently makes it impossible to obtain an analytical expression for the cell velocity in the DEP-FFF chamber at low applied voltages.

Despite these limitations of Eq. 14, our experimental data completely support the conclusion that cell velocity depends on the parameters $\text{Re}(f_{\text{CM}})$ and the applied voltage U (as shown in Eq. 14), when the DEP force is sufficiently large for the ill-defined hydrodynamic lift effects to be ignored. Thus, when we fitted Eq. 14 to the experimentally observed voltage dependency of the cell velocity shown in Fig. 6, good agreement between theory and experiment was found, with regression coefficients exceeding 0.99 for all three flow rates examined, even though each data point was derived from measurements on a different set of cells. At applied voltages below 0.2 V (RMS), however, the observed cell velocities were systematically larger than predicted by theory, principally as a result, we believe, of the ill-defined hydrodynamic lift effects.

Cell dielectric properties

When we extended our analysis in terms of Eq. 14 to the dependencies of cell velocity on the applied field frequency (see Fig. 5), using values of $\mathrm{Re}(f_{CM})$ calculated with the single-shell dielectric model of the cells (Irimajiri et al., 1979; Huang et al., 1992), a reasonably good fit was also achieved with the following parameters derived: the mean membrane capacitance and conductance of 15.6 mF/m^2 and 220 S/m^2, respectively. These values are in good agreement with those reported previously from electrorotation measurements of HL-60 cells (Becker et al., 1994). The frequency dependency of $\mathrm{Re}(f_{CM})$ based on the single-shell dielectric model is shown in Fig. 10. In the frequency range 5–50 kHz, despite the reduction of magnitude of $\mathrm{Re}(f_{CM})$ from −0.48 to −0.32, HL-60 cell velocities increased with frequency because of the increasing cell levitation height resulting from the diminishing electrode polarization effect discussed earlier. In the frequency range 50–100 kHz, $\mathrm{Re}(f_{CM})$ gradually decreased its negative magnitude to zero, and this resulted in a sharp decrement in HL-60 cell velocities. As the frequency increased above 100 kHz, $\mathrm{Re}(f_{CM})$ became positive for many cells, and these cells were attracted vertically toward the electrode plane and horizontally toward the electrode edges. As a result, cell heights above the electrode plane and the corresponding cell velocities became even smaller than those observed in the absence of an applied field. Thus it is also possible to utilize positive DEP forces in balance with the hydrodynamic lift and gravitational forces to control particle heights and velocities in a FFF application. Indeed, the concept of employing positive DEP forces to attract particles toward the bottom wall of a flow chamber to realize FFF was suggested and demonstrated by Washizu et al. (1994) in their studies of DNA molecules.

We observed that individual HL-60 cells exhibited a wide spread in velocities at 100 kHz, where the parameter $\mathrm{Re}(f_{CM})$ was close to zero. Because of the inhomogeneous nature of HL-60 cell cultures (a typical characteristic of transformed cell populations), a spread of cell dielectric properties and a corresponding spread of values of $\mathrm{Re}(f_{CM})$ occurred within each sample. Thus the membrane-specific capacitance of individual HL-60 cells in a typical culture was spread over the range of 13–20 mF/m^2, as determined from electrorotation measurements,. As shown in Fig. 9, two cells with the same density but $\mathrm{Re}(f_{CM})$ values of −0.01 and −0.02, respectively, had velocities that differed by 45%. For this reason, small differences in $\mathrm{Re}(f_{CM})$ between individual HL-60 cells in the culture population resulted in large variations in their DEP-FFF velocities at 100 kHz. This demonstrates that, when $\mathrm{Re}(f_{CM})$ is close to zero, cell velocities are very sensitive to cell dielectric properties. As a result, the DEP-FFF method has the potential for extremely sensitive discrimination between cell subpopulations with very subtle dielectric differences, and therefore represents an important advance over earlier DEP retention approaches to cell separation that require relatively large differences in cell dielectric properties.

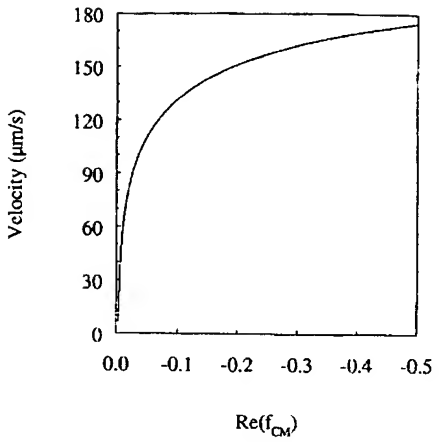

FIGURE 9 Dependence of the cell velocity on $\mathrm{Re}(f_{CM})$ in a DEP-FFF chamber as calculated using Eq. 14 with the following parameters: $\langle v \rangle$ = 200 μm/s; H = 200 μm; ρ_c = 1.089; ρ_m = 1.033 g/cm^3, $p(f)$ = 1, radius r = 5.8 μm. DEP forces are assumed to be generated by a parallel microelectrode of 20 μm width and spacing, with an applied voltage of 1 V RMS, so that d = 80 μm and $A = -2.77 \times 10^{14}$ m^{-3}.

Separation mechanics

To analyze dielectrophoretic forces acting on HL-60 and PBMN cells (mainly T- and B-lymphocytes) in the separation experiments, we calculated the typical frequency dependencies of $\mathrm{Re}(f_{CM})$ (Fig. 10) for HL-60 and T-lymphocytes, based on the mean values of their dielectric

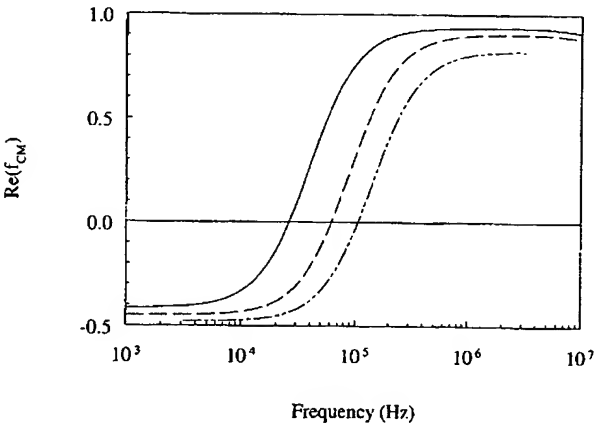

FIGURE 10 Simulated frequency dependencies of $\mathrm{Re}(f_{CM})$ for HL-60 cells (— · · —) in a suspending medium of conductivity 44 mS/m, and HL-60 cells (——) and T-lymphocytes (— —) in a suspending medium of conductivity 10 mS/m. The simulations were based on the mean values of dielectric parameters for the cells determined from electrorotational measurements. For HL-60 cells, membrane capacitance = 15.6 mF/m^2; membrane conductance = 220 S/m^2; cell interior conductivity = 0.75 S/m and relative permittivity = 75; radius = 5.8 μm. For T-lymphocytes, membrane capacitance = 11 mF/m^2; membrane conductance = 220 S/m^2; cell interior conductivity = 0.75 S/m and permittivity = 75; radius = 3.2 μm.

parameters determined by the electrorotation technique (Becker et al., 1994).

We showed previously (Becker et al., 1995) that the condition for separating two dissimilar cell types by the DEP retention approach is that the DEP forces on one cell type at the electrode edges prevail against the horizontal drag of eluate fluid flow and cause the cells to be retained, while the DEP forces acting on the other cell type(s) are weak and allow these cells to be eluted. In the case of retention of HL-60 cells and elution of PBMN cells, the condition can be written as

$$r_{HL}\,\mathrm{Re}(f_{CM})|_{HL}k_{DEPx\_HL} > \frac{61\pi\eta\langle v\rangle}{H\epsilon_m V^2} > r_{PBMN}\,\mathrm{Re}(f_{CM})|_{PBMN}k_{DEPx\_PBMN} \quad (15)$$

where η is the dynamic viscosity of the eluate, and k_{DEPx_HL} and k_{DEPx_PBMN} are the maximum horizontal components of the field nonuniformity factor ∇E^2_{RMS} arising from excitation of the electrode array for HL-60 and PBMN cells, respectively. At an applied frequency of 50 kHz, the $\mathrm{Re}(f_{CM})$ values for HL-60 and T-lymphocytes in Fig. 10 were 0.42 and −0.11, respectively. By adjusting the eluate flow rate to 160 μl/min, we were then able to satisfy the above inequality (Eq. 15). Under these conditions, the DEP force on the HL-60 cells was strongly attractive and exceeded the horizontal fluid drag by a factor of 3.5 (calculated using the simulated values for the field parameter k_{DEPx}), resulting in their entrapment. By contrast, the DEP forces on PBMN cells were repulsive, causing them to be flushed away.

For DEP-FFF separation, the field frequency was reduced to 25 kHz, at which frequency $\mathrm{Re}(f_{CM})$ for HL-60 cells and T-lymphocytes had the values −0.027 and −0.34, respectively. The DEP-levitation heights predicted by Eq. 10 for these $\mathrm{Re}(f_{CM})$ values are 33 and 17 μm for T-lymphocytes and HL-60 cells, respectively. Under these conditions, Eqs. 5 and 6 then predict that T-lymphocytes should travel about twice as fast as HL-60 cells, in good agreement with our experimental observation. To further illustrate the difference in elution velocities between HL-60 and PBMN cells, we determined their frequency dependencies under identical conditions (Fig. 11). At the low frequency of 10 kHz, the velocities of HL-60 and PBMN cells were quite similar, suggesting that they were positioned at similar heights. Above 20 kHz, HL-60 cells exhibited a sharp drop in velocities, until at 35 kHz they were retained at the electrode edges. In contrast, PBMN cells had near-constant velocities between 10 and 35 kHz, until above 40 kHz their velocity decreased, and all of the cells were trapped at electrode edges above 70 kHz.

Separation of HL-60 from PBMN cells in both DEP retention and DEP-FFF is based on differential DEP forces resulting from differences between $\mathrm{Re}(f_{CM})$ values of the different cell types. It has been well established (Glaser and Fuhr, 1987; Gascoyne et al., 1992; Wang et al., 1994) that membrane electrical properties dominate cell dielectrophoretic responses in the low-frequency range, where we have operated the DEP retention and DEP-FFF experiments. Indeed, using the electrorotation method, we have previously determined that the mean membrane capacitances of HL-60 and T-lymphocytes were 15 and 11 mF/m^2, respectively (Becker et al., 1994). Thus it was the difference in membrane capacitive characteristics that served as the basis for the separation and discrimination of HL-60 cells and PBMN cells in these DEP retention and DEP-FFF studies.

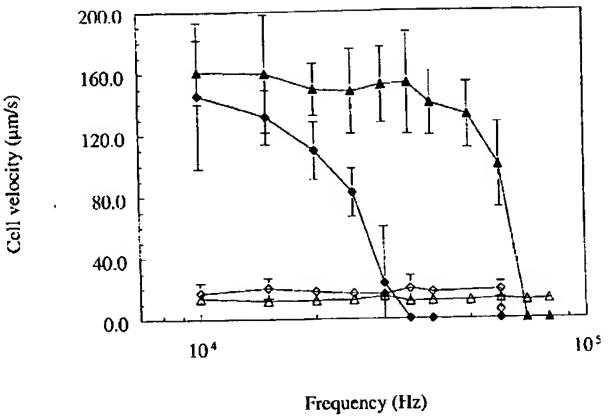

FIGURE 11 Frequency dependencies of the mean velocities for HL-60 (♦) and PBMN (▲) cells suspended in a sucrose/dextrose medium of conductivity 10 mS/m in a thin chamber containing parallel microelectrode arrays (50 μm width and spacing) for a flow rate of 160 μl/min ($\langle v\rangle$ = 392 μm/s). The applied voltage was 0.88 V (RMS). The chamber dimensions were 375 μm (H) × 150 mm (L) × 24 mm (W). Each point represents the mean velocity of more than 15 cells. The open symbols correspond to the cell velocities when the electrical field was turned off.

CONCLUSIONS AND PERSPECTIVE

We have reported a new technique for cell characterization and separation that combines dielectrophoretic levitation and field-flow fractionation. In this method, an inhomogeneous dielectrophoretic-levitation force acts to balance the homogeneous gravitational force, and provides an effective mechanism for controlling positions of cells and their corresponding velocities in a fluid flow profile. Thus cell velocities and their corresponding transit time across a DEP-FFF chamber directly reflect their individual dielectric characteristics and can be exploited for both characterization and separation purposes.

Using HL-60 cells in thin chambers equipped with parallel electrode arrays on their bottom walls, we demonstrated the validity of a theoretical model for the DEP-FFF system. The cell levitation height and corresponding velocity in an eluate flow profile were shown to be very sensitive to cell dielectric properties, especially when the parameter $\mathrm{Re}(f_{CM})$ was close to zero. This ability is significant for biological and clinical problems in which cell subpopula-

tions with subtle differences must be separated. Finally, we demonstrated that HL-60 cells could be separated from normal PBMN cells by using both DEP-FFF and DEP retention approaches.

As shown in Eq. 7, the electric field distribution $q(h)$ critically determines the sensitivity of the dependence of cell levitation height, and thus traveling velocity, on cell dielectric properties. We are directing efforts toward the design of electrode geometries that provide optimized field distributions for various applications. Further studies are also needed to improve our understanding of the nature of the hydrodynamic lift effect.

We thank Carrie Hamilton and Jamileh Noshari for cell culture work, and Giovanni De Gasperis, Jody Vykoukal, Xujing Wang, and Jun Yang for valuable discussions.

This work is supported in part by National Institutes of Health grant R01 DK51065-01 from the National Institute of Diabetes and Digestive and Kidney Disease, a Biomedical Engineering Research grant from the Whitaker Foundation, and a Crockrell Foundation UCF Scientific Achievement Fellowship.

REFERENCES

Andreux, J. P., A. Merino, M. Renard, F. Forestier, and Ph. J. P. Cardot. 1993. Separation of red blood cells by field flow fractionation. *Exp. Hematol.* 21:326–330.

Becker, F. F., X-B. Wang, Y. Huang, R. Pethig, J. Vykoukal, and P. R. C. Gascoyne. 1994. The removal of human leukemia cells from blood using interdigitated microelectrodes *J. Phys. D Appl. Phys.* 27:2659–2662.

Becker, F. F., X-B. Wang, Y. Huang, R. Pethig, J. Vykoukal, and P. R. C. Gascoyne. 1995. Separation of human breast cancer cells from blood by differential dielectric affinity. *Proc. Natl. Acad. Sci. USA.* 92:860–864.

Berg, H. C., and L. Turner. 1991. Selection of motile nonchemotactic mutants of *Escherichia coli* by field-flow fractionation. *Proc. Natl. Acad. Sci. USA.* 88:8145–8148.

Boyum, A. 1974. Separation of blood leucocytes, granulocytes and lymphocytes. *Tissue Antigens.* 4:269–274.

Cardot, Ph. J. P., C. Elgea, M. Guernet, D. Godet, and J. P. Andreux. 1994. Size- and density-dependent elution of normal and pathological red blood cells by gravitational field-flow fractionation. *J. Chromatogr.* 654B:193–203.

Chess, L., and S. F. Schlossman. 1976. Anti-immunoglubulin columns and the separation of T, B, and null cells. *In* In Vitro Methods in Cell Mediated and Tumor Immunity. B. R. Bloom and J. R. David, editors. Academic, New York. 255–261.

Cox, R. G., and S. K. Hsu. 1977. The lateral migration of solid particles in a laminar flow near a plane. *Int. J. Multiphase Flow.* 3:201–222.

Fischer, A. 1993. The use of monoclonal antibodies in allogeneic bone marrow transplantation. *Br. J. Haematol.* 83:531–534.

Fuhr, G., W. M. Arnold, R. Hagedorn, T. Muller, W. Benecke, B. Wagner, and U. Zimmermann. 1992. Levitation, holding, and rotation of cells within traps made by high-frequency fields. *Biochim. Biophys. Acta.* 1108:215–223.

Fuhr, G., U. Zimmermann, and S. G. Shirley. 1996. Cell motion in time-varying fields: principles and potential. *In* Electromanipulation of Cells. U. Zimmermann and G. A. Neil, editors. CRC Press, Boca Raton, FL. 260–328.

Gascoyne, P. R. C., Y. Huang, R. Pethig, J. Vykoukal, and F. F. Becker. 1992. Dielectrophoretic separation of mammalian cells studied by computerized image analysis. *Meas. Sci. Technol.* 3:439–445.

Gascoyne, P. R. C., Y. Huang, X.-J. Wang, J. Yang, G. DeGasperis, and X.-B. Wang. 1996. Cell separation by conventional dielectrophoresis combined with field-flow-fractionation. *Biophys. J.* 70:A333.

Giddings, J. C. 1989. Field-flow fractionation of marcromolecules. *J. Chromatogr.* 470:327–335.

Giddings, J. C. 1993. Field-flow fractionation: analysis of macromolecular, colloidal, and particulate materials. *Science.* 260:1456–1465.

Glaser, R., and G. Fuhr. 1987. Electrorotation—the spin of cells in rotating high frequency electric fields. *In* Mechanistic Approaches to Interactions of Electric and Electromagnetic Fields with Living Systems. M. Blank and E. Findl, editors. Plenum Press, New York. 271–290.

Goldman, A. J., R. G. Rox, and H. Brenner 1967. Slow viscous motion of a sphere parallel to a plane wall. II. Couette flow. *Chem. Eng. Sci.* 22:653–660.

Huang, Y., R. Holzel, R. Pethig, and X.-B. Wang. 1992. Differences in the AC electrodynamics of viable and non-viable yeast cells determined through combined dielectrophoresis and electrorotation studies. *Phys. Med. Biol.* 37:1499–1517.

Irimajiri, A., T. Hanai, and A. Inouye. 1979. A dielectric theory of "multi-stratified shell" model with its application to a lymphoma cell. *J. Theor. Biol.* 78:251–269.

Jones, T. B. 1979. Dielectrophoretic force calculation. *J. Electrostat.* 6:69–82.

Kaler, K. V. I. S., and T. B. Jones. 1990. Dielectrophoretic spectra of single cells determined by feedback-controlled levitation. *Biophys. J.* 57: 173–182.

Leighton, D., and A. Acrivos. 1985. The lift on a small sphere touching a plane in the presence of a simple shear flow. *J. Appl. Math. Phys.* 26:174–178.

Litzen, A., J. K. Walter, H. Krischollek, and K.-G. Wahlund. 1993. Separation and quantitation of monoclonal antibody aggregates by asymmetrical flow field-flow fractionation and comparison to gel permeation chromatography. *Anal. Biochem.* 212:469–480.

Markx, G. H., Y. Huang, X. F. Zhou, and R. Pethig. 1994a. Dielectrophoretic characterization and separation of micro-organisms. *Microbiology.* 140:585–591.

Markx, G. H., and R. Pethig. 1995. Dielectrophoretic separation of cells: continuous separation. *Biotech. Bioeng.* 45:337–343.

Markx, G. H., M. Talary, and R. Pethig. 1994b. Separation of viable and non-viable yeast using dielectrophoresis. *J. Biotechnol.* 32:29–37.

Mosersky, S. M., K. D. Caldwell, S. B. Jones, B. E. Maleeff, and R. A. Barford. 1988. Sedimentation field flow fractionation of mitochondrial and microsomal membranes from corn roots. *Anal. Biochem.* 172: 113–123.

Pohl, H. 1977. Dielectrophoresis: application to the characterization and separation of cells. *In* Methods of Cell Separation. Vol. I. N. Catsimpoolas, editor. Plenum Press, New York. 67–169.

Sadiku, M. N. O. 1996. Numerical Techniques in Electromagnetics, ch. 5, Moment Methods. CRC Press, Boca Raton, FL. 309–406.

Schwan, H. P. 1992. Linear and nonlinear electrode polarization and biological materials. *Ann. Biomed. Eng.* 20:269–288.

Smeland, E. B., S. Funderud, H. K. Blomhoff, and T. Egeland. 1992. Isolation and characterization of human hematopoietic progenitor cells: an effective method for the positive selection of CD34(+) cells. *Leukemia.* 6:845–852.

Talary, M., K. I. Mills, T. Hoy, A. K. Burnett, and R. Pethig. 1995. Dielectrophoretic separation and enrichment of CD34+ cell subpopulation from bone marrow and peripheral blood stem cells. *Med. Biol. Eng. Comp.* 33:235–237.

Wang, X., X.-B. Wang, F. F. Becker, and P. R. C. Gascoyne. 1996. A theoretical method of electrical field analysis for dielectrophoretic electrode arrays using Green's theorem. *J. Phys. D Appl. Phys.* 29: 1649–1660.

Wang, X.-B., Y. Huang, F. F. Becker, and P. R. C. Gascoyne. 1997. Dielectrophoretic manipulation of cells using spiral electrodes. *Biophys. J.* 72:1887–1899.

Wang, X.-B., Y. Huang, J. P. H. Burt, G. H. Markx, and R. Pethig. 1993. Selective dielectrophoretic confinement of bioparticles in potential energy wells. *J. Phys. D Appl. Phys.* 26:1278–1285.

Wang, X.-B., Y. Huang, P. R. C. Gascoyne, F. F. Becker, R. Holzel, and R. Pethig. 1994. Changes in Friend murine erythroleukaemia cell mem-

branes during differentiation determined by electrorotation. *Biochim. Biophys. Acta.* 1193:330–344.

Wang, X.-B., M. P. Hughes, Y. Huang, F. F. Becker, and P. R. C. Gascoyne. 1995. Non-uniform spatial distributions of both the magnitude and phase of AC electric fields determine dielectrophoretic forces. *Biochim. Biophys. Acta.* 1234:185–194.

Washizu, M., and T. B. Jones. 1996. Generalized multipolar dielectrophoretic force and electrorotational torque calculation. *J. Electrostat.* 37:121–134.

Washizu, M., S. Suzuki, O. Kurosawa, T. Nishizaka, and T. Shinohara. 1994. Molecular dielectrophoresis of biopolymers. *IEEE Trans. Ind. Appl.* 30:835–843.

Williams, P. S., T. Koch, and J. C. Giddings. 1992. Characterization of near-wall hydrodynamic lift forces using sedimentation field-flow fractionation. *Chem. Eng. Comm.* 111:121–147.

Zhou, X.-F., G. H. Markx, R. Pethig, and I. E. Eastwood. 1995. Differentiation of viable and non-viable bacterial biofilm using electrorotation. *Biochim. Biophys. Acta.* 1245:85–93.